

# A digital technique for art authentication

Siwei Lyu\*, Daniel Rockmore\*<sup>†</sup>, and Hany Farid\*\*<sup>‡</sup>

Departments of \*Computer Science and <sup>†</sup>Mathematics, Dartmouth College, Hanover, NH 03755

Communicated by David L. Donoho, Stanford University, Stanford, CA, September 1, 2004 (received for review May 13, 2004)

**We describe a computational technique for authenticating works of art, specifically paintings and drawings, from high-resolution digital scans of the original works. This approach builds a statistical model of an artist from the scans of a set of authenticated works against which new works then are compared. The statistical model consists of first- and higher-order wavelet statistics. We show preliminary results from our analysis of 13 drawings that at various times have been attributed to Pieter Bruegel the Elder; these results confirm expert authentications. We also apply these techniques to the problem of determining the number of artists that may have contributed to a painting attributed to Pietro Perugino and again achieve an analysis agreeing with expert opinion.**

It probably was not long after people began paying money for art that a lucrative business in forging art was born, and it probably was not too much later that techniques for detecting art forgeries emerged. Even today, the early techniques for authentication remain preeminent. By and large, these techniques are based on “connoisseurship” and so rely on the discerning eyes of a few experts who are steeped in the work and life of the artist in question. Their opinion may be informed by the “*catalogue raison*,” which is the current acknowledged authoritative work on the artist’s oeuvre. Other desiderata may include provenance that might be traced back to the artist’s circle or his collectors and makes possible the comparison of the work’s implicit biography with the histories of related works or even a detailed analysis of any signature that may be present. (See ref. 1 for a survey of current techniques.)

In addition to the reliance on the human actor, quantitative methods can be brought to bear. X-ray analysis can reveal a painting beneath a painting that can shed light on its origins. Surface analysis of the painting materials is another approach, most famously applied in the investigation of the famous “van Meerghe forgeries.” In this case, the forgery of paintings attributed to Johannes Vermeer was confirmed by dating the paintings according to the proportion of a certain lead isotope in the lead-based paint. An elementary application of differential equations allowed for the actual isotope content to be compared with the expected content had the work been painted in Vermeer’s day (2). This technique marked a first use of mathematics in the service of art authentication.

With the advent of powerful digital technology, computational tools may be able to provide new insights into and techniques for the art and science of art authentication. For example, a fractal analysis of Jackson Pollock’s drip paintings has revealed interesting relations between the evolution of Pollock’s aesthetic and the fractal dimension of his work (3, 4). The analysis also raises the possibility of using fractal dimension to help authenticate work attributed to Pollock. Various techniques from machine learning have been applied to the analysis and classification of “*craquelure*,” the crack lines that appear over time in a painting (5).

In this paper we present a computational tool for analyzing prints, drawings, and paintings for use in authentication. Specifically, we performed a multiscale, multiorientation image decomposition (e.g., wavelets) of a collection of high-resolution digital scans of a drawing or painting. This decomposition changes the basis from functions maximally localized in space (pixels) to one in which the basis functions are localized not only in space but also in orientation and scale. A familiar analogy comes from sound, where the original sound might be transformed into a vector of local

frequency information that reflects how much of each frequency comprises the original sound over a short time window. We constructed a compact model of the statistics from such a multiscale, multiorientation image decomposition, and we looked for consistencies or inconsistencies across different drawings or paintings or within a single work. The latter is the so-called “problem of many hands” in which we try to determine the regions of a collaborative work that have been accomplished by a single artist.

The analysis produced locally oriented spatial frequency data and so suggests that the accompanying model captures the subtle pen and brush strokes characteristic of an artist. Although an imitation<sup>§</sup> may be perceptually similar to an original (i.e., very much in the “style of the master”), the subtle differences in stroke can reveal the presence of an imitation. In a sense, this work is a natural successor to the mathematical techniques used for graphology, or handwriting analysis (6), distilling not just the characteristic lines and curves of a painter’s literal signature (which is often part of the process of authentication) but, even more, moving toward a characterization of the artist’s aesthetic signature, resident within the line and curve of his or her work.

Analogous techniques already have made their way into the literary world, where they fall within the discipline of “stylometry” (7). The problem of classification has been applied to divvying up the attribution of The Federalist Papers between James Madison and Alexander Hamilton (8) and the determination of the authorship of the 15th book in the Oz series (9). Statistical approaches to the question of authentication have surfaced in the analysis of William Shakespeare’s sonnets (10). The problem of many hands finds its mirror in a study of the conjectured multiple authorship of the Old Testament (11).

We began by applying our analysis to the problem of authentication of a collection of 13 drawings that have at one time been attributed to the famous draftsman Pieter Bruegel the Elder. We followed with a “many-hands” analysis of a portrait by the great Renaissance painter Perugino. We closed with a synopsis of the tools used in the analysis and described the underlying statistical model. We collected some of the more technical points in an appendix.

## Materials

**Bruegel.** The Flemish painter and draftsman Pieter Bruegel the Elder (1525/30–1569) was among the greatest artists of the 16th century. Of particular beauty and fame are Bruegel’s landscape drawings. Over time he acquired many imitators; undoubtedly some simply were eager to work in the style of the great master, whereas others surely were hoping to pass off their work as Bruegel’s for monetary gain. Some of these followers and imitators were expert enough that after being unmasked (or discovered) they became famous in their own right, e.g., Jacob Savery. Bruegel’s work recently has been the subject of renewed study and interest (12–14).

Abbreviation: MDS, multidimensional scaling.

<sup>†</sup>To whom correspondence should be addressed at: 6211 Sudikoff Laboratory, Department of Computer Science, Dartmouth College, Hanover, NH 03755. E-mail: farid@cs.dartmouth.edu.

<sup>§</sup>Henceforth we will give the benefit of the doubt to the imitator and use the term “imitation” rather than the more charged “forgery.”

© 2004 by The National Academy of Sciences of the USA

**Table 1. Authentic and imitation works of art**

MMA cat. no.	Title	Artist
Authentic		
3	Pastoral Landscape	Bruegel
4	Mountain Landscape with Ridge and Valley	Bruegel
5	Path through a Village	Bruegel
6	Mule Caravan on Hillside	Bruegel
9	Mountain Landscape with Ridge and Travelers	Bruegel
11	Landscape with Saint Jerome	Bruegel
13	Italian Landscape	Bruegel
20	Rest on the Flight into Egypt	Bruegel
Imitation		
7	Mule Caravan on Hillside	—
120	Mountain Landscape with a River, Village, and Castle	—
121	Alpine Landscape	—
125	Sollicitudo Rustica	—
127	Rocky Landscape with Castle and a River	Savery

The first column corresponds to the Metropolitan Museum of Art (MMA) catalog number in ref. 13. —, unknown.

As a result, many drawings formerly attributed to Bruegel now are attributed to others (Table 1).

The delicate line and shading characterizing these works suggests that their classification according to a wavelet-like analysis may be both appropriate and fruitful. For our analysis we digitally scanned (at 2,400 dots per inch) eight authenticated drawings by Bruegel and five acknowledged Bruegel imitations from 35-mm color slides (Table 1), which were provided courtesy of the Metropolitan Museum of Art, New York (13). These color [red, green, blue (RGB)] images, originally  $3,894 \times 2,592$  pixels, were cropped to a central  $2,048 \times 2,048$ -pixel region, converted to grayscale<sup>1</sup> (gray = 0.299 R + 0.587 G + 0.114 B), and autoscaled to fill the full intensity range [0,255]. Fig. 1 shows examples of an authentic drawing and an imitation.

Each digital image then was subdivided into 64 nonoverlapping  $256 \times 256$ -pixel regions. Each of these subimages then was transformed by using a five-level, three-orientation wavelet-like decomposition (see *Methods* for details). From this decomposition, a 72 feature vector of coefficient and error statistics was extracted for each subimage (see *Methods*). Each drawing then corresponded to a set of points in this 72-dimensional space. Authentication was indicated by the distance between these point clouds, with the belief that works by the same artist would be close together, irrespective of content, and that an imitation would be relatively far from the authenticated Bruegels. Thus, we first computed the Hausdorff distance (15) between all pairs of images (see *Appendix A*). The resulting  $13 \times 13$  distance matrix then was subjected to a multidimensional scaling [(MDS) ref. 16] (see *Appendix B*). Fig. 1 shows the result of visualizing the original 13 images in a lower-dimensional space as determined by a MDS analysis.

The circles in Fig. 1 correspond to the authentic drawings, and the squares correspond to the imitations. For purposes of visualization, the wire-frame sphere was rendered at the center of mass of the eight authenticated drawings and with a radius set to fully encompass all eight data points (in so doing, we assume knowledge of the authenticated Bruegels). Note that all five

<sup>1</sup>Although converting from color to grayscale results in a significant loss of information, we did so to make it more likely that the measured statistical features and subsequent classification were more likely to be based on the artist's strokes and not on simple color differences.

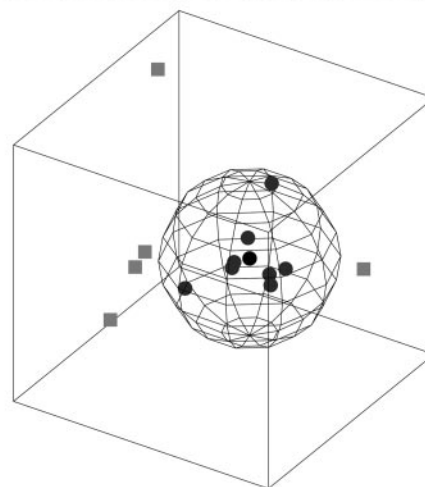


**Fig. 1.** Authentic works by Bruegel and imitations. An authentic work (*Top*) and an imitation (*Middle*) (nos. 6 and 7, respectively, in Table 1). (*Bottom*) The results of analyzing eight authentic Bruegel drawings (●) and five imitations (■). Note how the imitations lie significantly outside the bounding sphere of authentic drawings.

imitations fall well outside the sphere. The distances from the authenticated Bruegels to the center of the sphere are 0.34, 0.35, 0.55, 0.90, 0.56, 0.17, 0.54, and 0.85. The distances from the imitations are considerably larger, at 1.58, 2.20, 1.90, 1.48, and 1.33 (the difference in the means of these two distance populations is statistically significant:  $P < 1^{-5}$ , one-way ANOVA). Even in this space of reduced dimension, there is a clear difference between the authentic drawings and the imitations.

**Perugino.** Pietro di Cristoforo Vannucci (Perugino) (1446–1523) is well known as a portrait and a fresco painter, but perhaps he is best known for his altarpieces. By the 1490s, Perugino maintained workshops in Florence and Perugia, Italy, and he was quite prolific. Shown in Fig. 2 is the painting “Madonna with

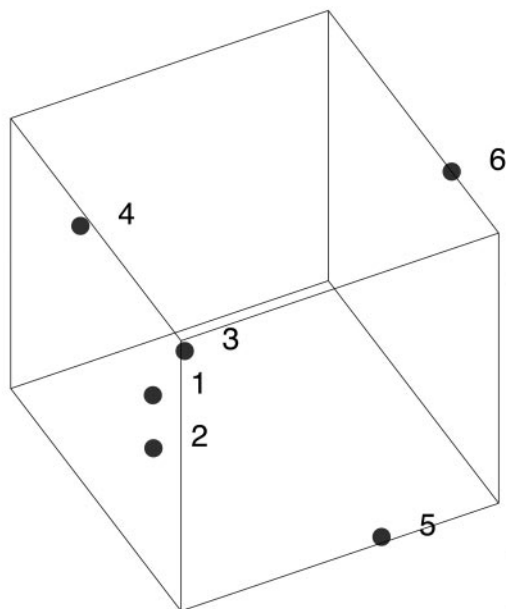
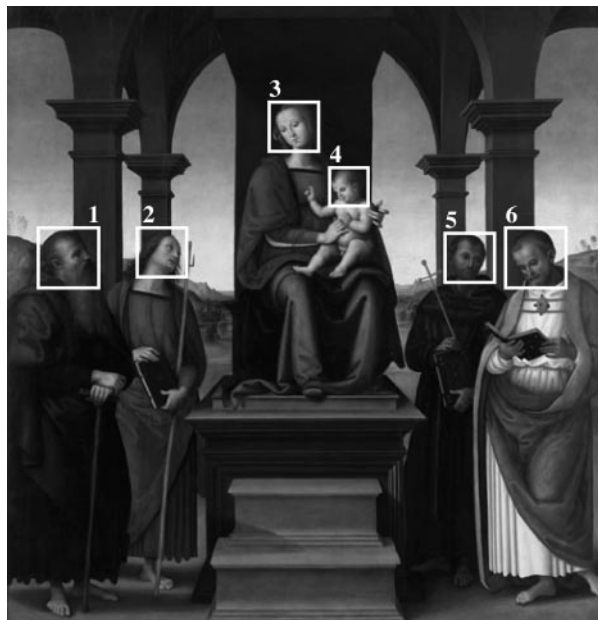


**Fig. 2.** How many hands contributed to this painting? (Upper) “Madonna with Child” by Perugino. (Lower) The results of analyzing the Perugino painting. The numbered data points correspond to the six faces (from left to right). Note how the three leftmost faces (1–3) cluster, whereas the remaining faces (4–6) are distinct. This clustering pattern suggests the presence of at least four distinct hands.

Child” by Perugino. As with many of the great Renaissance paintings, however, it is likely that Perugino only painted a portion of this work, and apprentices did the rest. To this end, we wondered whether we could uncover statistical differences among the faces of the individual characters.

The painting (at the Hood Museum of Art, Dartmouth College) was photographed by using a large-format camera ( $8 \times 10$ -inch negative) and drum-scanned to yield a color  $16,852 \times 18,204$ -pixel image. As in the previous section, this image was converted to grayscale. The facial region of each of the six characters was manually localized. Each face then was partitioned into nonoverlapping  $256 \times 256$ -pixel regions and autoscaled into the full-intensity range (0, 255). This partitioning yielded (from left to right)

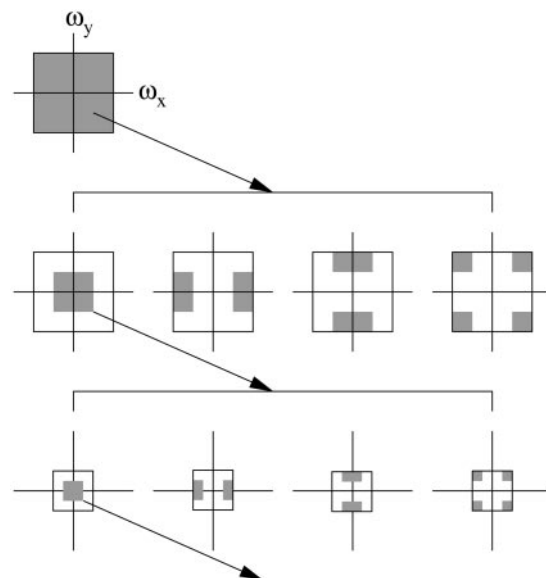


**Fig. 3.** An idealized multiscale and orientation decomposition of frequency space. From top to bottom, levels are 0, 1, and 2. From left to right are low-pass, vertical, horizontal, and diagonal subbands.

189, 171, 189, 54, 81, and 144 regions. The same set of statistics described in the previous section was collected from each of these regions. Also as in the previous section, we computed the Hausdorff distance (see *Appendix A*) between all pairs of six faces. The resulting  $6 \times 6$  distance matrix then was subjected to MDS (see *Appendix B*). Fig. 2 shows the result of visualizing the original six faces in a lower-dimensional space as determined by a MDS analysis.

The numbered data points correspond to the six faces (from left to right) in Fig. 2. Note how the three leftmost faces cluster, whereas the remaining faces are distinct. The average distance between faces 1–3 is 0.61, whereas the average distance between the other faces is 1.79. This clustering pattern suggests the presence of at least four distinct hands and is consistent with the views of some art historians (T. Barton Thurber, Hood Museum, Dartmouth College, personal communication).

## Methods

Our methodology makes use of a decomposition of images by using basis functions that are localized in spatial position, orientation, and scale (e.g., wavelets). These sorts of expansions have proven extremely useful in a range of applications (e.g., image compression, image coding, noise removal, and texture synthesis). One reason for this utility is that such decompositions exhibit statistical regularities that can be exploited (17–19). Described below is one such decomposition and a set of statistics collected from this decomposition.<sup>||</sup>

The decomposition is based on separable quadrature mirror filters (20–22). As illustrated in Fig. 3, this decomposition splits the frequency space into multiple scales and orientations. This decomposition is accomplished by applying separable low-pass and high-pass filters along the image axes, generating a vertical, horizontal, diagonal, and low-pass subband. For example, the horizontal subband is generated by convolving with the high-pass filter in the horizontal direction and the low-pass filter in the vertical direction,

<sup>||</sup>We also have experimented with both Laplacian and steerable pyramid decompositions. Results from a steerable pyramid (with eight orientation subbands) were similar to the results included above (which use only three orientation subbands). Furthermore, the Laplacian pyramid generally gave poor results. So, although it seems that oriented subbands are necessary, it also seems that a finer tuning of orientation is not necessary for this particular task.

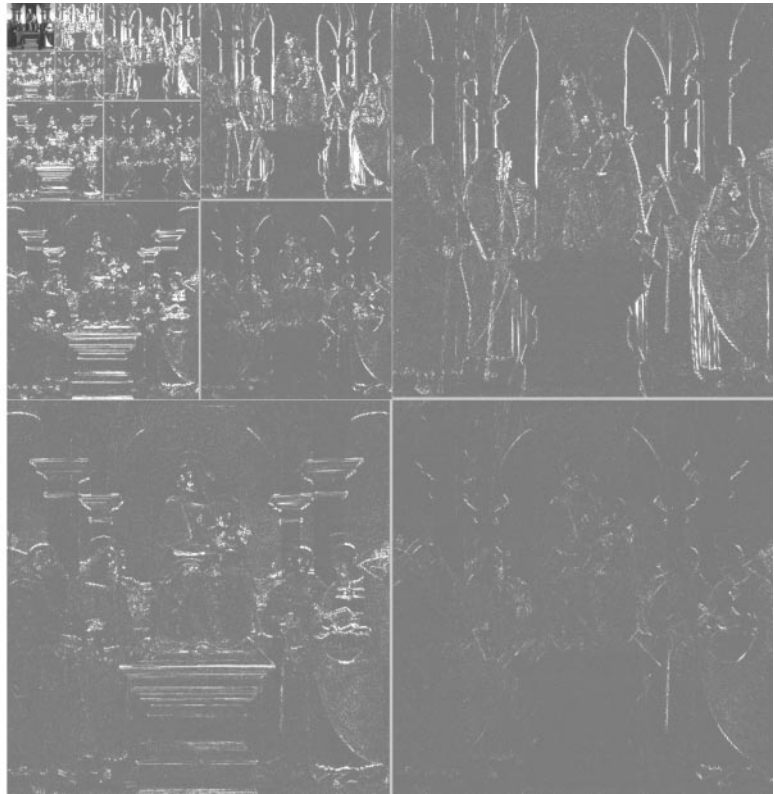


**Fig. 4.** The absolute values of the subband coefficients at three scales and three orientations (the residual low-pass subband is shown in the upper left corner) (Right) for the Perugino painting (Left).

the diagonal band is generated by convolving with the high-pass filter in both directions, etc. Subsequent scales are created by subsampling the low-pass subband by a factor of two and recursively filtering. The vertical, horizontal, and diagonal subbands at scale  $i = 1, \dots, n$  are denoted as  $V_i(x, y)$ ,  $H_i(x, y)$ , and  $D_i(x, y)$ , respectively. Fig. 4 Right and Left shows a three-level decomposition of the scanned Perugino work, respectively.

Given this image decomposition, the statistical model is composed of the mean, variance, skewness, and kurtosis of the subband coefficients at each orientation and at scales  $i = 1, \dots, n - 2$ . These statistics characterize the basic coefficient distributions. To capture the higher-order correlations that exist within this image decomposition, these coefficient statistics are augmented with a set of statistics based on the errors in an optimal linear predictor of coefficient magnitude.

As described in ref. 19, the subband coefficients are correlated to their spatial, orientation, and scale neighbors. For purposes of illustration, consider first a vertical band,  $V_i(x, y)$ , at scale  $i$ . A linear predictor for the magnitude of these coefficients in a subset of all possible neighbors may be given by

$$\begin{aligned}
 |V_i(x, y)| = & w_1|V_i(x - 1, y)| + w_2|V_i(x + 1, y)| \\
 & + w_3|V_i(x, y - 1)| + w_4|V_i(x, y + 1)| \\
 & + w_5|V_{i+1}\left(\frac{x}{2}, \frac{y}{2}\right)| + w_6|D_i(x, y)| \\
 & + w_7|D_{i+1}\left(\frac{x}{2}, \frac{y}{2}\right)|, \quad [1]
 \end{aligned}$$

where  $w_k$  denotes scalar weighting values, and  $|\cdot|$  denotes magnitude. This particular choice of spatial, orientation, and scale neighbors was used in our earlier work on detecting traces of

digital tampering in images.\*\* Here, we employed an iterative brute-force search (on a per-subband and per-image basis) for the set of neighbors that minimizes the prediction error within each subband.

Consider again the vertical band,  $V_i(x, y)$ , at scale  $i$ . We constrained the search of neighbors to a  $3 \times 3$  spatial region at each orientation subband and at three scales, namely, the neighbors

$$\begin{aligned}
 & V_i(x - c_x, y - c_y), H_i(x - c_x, y - c_y), \\
 & D_i(x - c_x, y - c_y), \\
 & V_{i+1}\left(\frac{x}{2} - c_x, \frac{y}{2} - c_y\right), H_{i+1}\left(\frac{x}{2} - c_x, \frac{y}{2} - c_y\right), \\
 & D_{i+1}\left(\frac{x}{2} - c_x, \frac{y}{2} - c_y\right), \\
 & V_{i+2}\left(\frac{x}{4} - c_x, \frac{y}{4} - c_y\right), H_{i+2}\left(\frac{x}{4} - c_x, \frac{y}{4} - c_y\right), \\
 & D_{i+2}\left(\frac{x}{4} - c_x, \frac{y}{4} - c_y\right),
 \end{aligned}$$

with  $c_x = \{-1, 0, 1\}$  and  $c_y = \{-1, 0, 1\}$ , and, of course, excluding  $V_i(x, y)$ . From these 80 possible neighbors, the iterative search begins by finding the single most predictive neighbor [e.g.,  $V_{i+1}(x/2 - 1, y/2)$ ].<sup>††</sup> This neighbor is held fixed, and the next

\*\*Farid, H. & Lyu, S. IEEE Workshop on Statistical Analysis in Computer Vision (in conjunction with Computer Vision and Pattern Recognition), June 17–23, 2003, Madison, WI.

††Integer rounding is used when computing the spatial positions of a parent, e.g.,  $x/2$  or  $x/4$ .

most predictive neighbor is found. This process is repeated five more times to find the optimally predictive neighborhood. On the  $k$ th iteration, the predictor coefficients  $(w_1, \dots, w_k)$  are determined as follows. Let the vector  $\vec{V}$  contain the coefficient magnitudes of  $V_i(x, y)$  strung out into a column vector, and the columns of the matrix  $Q$  contain the chosen neighboring coefficient magnitudes also strung out into column vectors. The linear predictor then takes the form

$$\vec{V} = Q\vec{w}, \quad [2]$$

where the column vector  $\vec{w} = (w_1, \dots, w_k)^T$ . The predictor coefficients are determined by minimizing the quadratic error function:

$$E(\vec{w}) = [\vec{V} - Q\vec{w}]^2. \quad [3]$$

This error function is minimized by differentiating with respect to  $\vec{w}$ :

$$dE(\vec{w})/d\vec{w} = 2Q^T[\vec{V} - Q\vec{w}], \quad [4]$$

setting the result equal to zero and solving for  $\vec{w}$  to yield

$$\vec{w} = (Q^T Q)^{-1} Q^T \vec{V}. \quad [5]$$

The log error in the linear predictor then is given by

$$\vec{E}_v = \log_2(\vec{V}) - \log_2(|Q\vec{w}|). \quad [6]$$

Once the full set of neighbors is determined, additional statistics are collected from the errors of the final predictor, namely, the mean, variance, skewness, and kurtosis. This entire process is repeated for each oriented subband, and at each scale  $i = 1, \dots, n - 2$ , where at each subband a new set of neighbors is chosen and a new linear predictor is estimated.

For an  $n$ -level pyramid decomposition, the coefficient statistics consist of  $12(n - 2)$  values, and the error statistics consist of another  $12(n - 2)$  values, for a total of  $24(n - 2)$  statistics. These values represent the measured statistics of an artist's style and are used to classify or cluster drawings or paintings.

As stated above, after the computation of the feature vectors, MDS was used to project the original 72-dimensional feature vectors into a three-dimensional subspace. Features with no discriminating power (e.g., the means) therefore will play no role in the lower-dimensional embedding.

## Discussion

We have presented a computational tool for digitally authenticating or classifying works of art. This technique looks for consistencies or inconsistencies in the first- and higher-order wavelet statistics collected from drawings or paintings (or por-

tions thereof). We showed preliminary results from our analysis of 13 drawings either by or in the style of Pieter Bruegel the Elder as well as a painting by Perugino. We expect these techniques, in collaboration with existing physical authentication, to play an important role in the field of art forensics.

## Appendix A: Hausdorff Distance

The Hausdorff distance is a distance metric defined on two sets of vectors,  $X$  and  $Y$ . The metric,  $H(\cdot, \cdot)$  is defined as

$$H(X, Y) = \max(h(X, Y), h(Y, X)),$$

where  $h(\cdot, \cdot)$  is defined as

$$h(X, Y) = \max_{\vec{x} \in X} \left( \min_{\vec{y} \in Y} d(\vec{x}, \vec{y}) \right).$$

Here  $d(\cdot, \cdot)$  can be any distance metric defined on the vector space subsuming  $X$  and  $Y$ . In our case, we use Euclidean distance  $d(\vec{x}, \vec{y}) = \sqrt{(\vec{x} - \vec{y})^T (\vec{x} - \vec{y})}$ .

## Appendix B: MDS

MDS is a popular method to visualize high-dimensional data. Given  $n$  vectors  $\{\vec{x}_1, \dots, \vec{x}_n\}$ , where  $\vec{x}_i \in \mathcal{R}^m$ , the goal of MDS is to find a lower-dimensional embedding for these data that minimally distorts their pairwise distances. Denote the  $n \times n$  distance matrix as  $D_{ij} = d(\vec{x}_i, \vec{x}_j)$ , where  $d(\cdot, \cdot)$  is a distance metric in  $\mathcal{R}^m$ . The most common such metric is Euclidean distance defined as  $d(\vec{x}_i, \vec{x}_j) = \sqrt{(\vec{x}_i - \vec{x}_j)^T (\vec{x}_i - \vec{x}_j)}$ .

Given the pairwise symmetric distance matrix, the classic (metric) MDS algorithm is given by the following steps:

1. Let  $A_{ij} = -\frac{1}{2} D_{ij}^2$ .
2. Let  $B = HAH$ , where  $H = I_n - \frac{1}{n} \vec{u}\vec{u}^T$ ,  $I_n$  is a  $n \times n$  identity matrix, and each component of the  $n$ -dimensional vector  $\vec{u}$  is 1.
3. Compute the eigenvectors,  $\vec{e}_1, \dots, \vec{e}_n$ , and corresponding eigenvalues,  $\lambda_1, \dots, \lambda_n$ , of matrix  $B$ , where  $\lambda_1 \geq \lambda_2 \geq \dots \geq \lambda_n$ .
4. The new, lower-dimensional representation of the original data,  $\vec{x}'_i$ , are then given by  $\vec{x}'_i = [\vec{e}_1(i) \vec{e}_2(i) \dots \vec{e}_{m'}(i)]$  where  $\vec{e}_k(i)$  denotes the  $i$ th component of the vector, and in our examples  $m' = 3$ .

We thank George Goldner and Nadine Orenstein of the Metropolitan Museum of Art and Kathy Hart of the Hood Museum of Art for their assistance and cooperation. D.R. was supported by Air Force Office of Scientific Research Grant F49620-00-1-0280. H.F. was supported by an Alfred P. Sloan Fellowship, National Science Foundation CAREER Grant IIS-99-83806, Department of Justice Grant 2000-DT-CS-K001, and departmental National Science Foundation Infrastructure Grant EIA-98-02068.

1. Spencer, R. D. (2004) *The Expert Versus the Object* (Oxford Univ. Press).
2. Keisch, B. (1968) *Science* **160**, 413–415.
3. Taylor, R., Micolich, A. P. & Jones, D. (1999) *Nature* **399**, 422.
4. Taylor, R. (2004) *Chaos Complexity Lett.*, in press.
5. Abas, F. S. & Martinez, K. (2003) *Proc. SPIE Int. Soc. Opt. Eng.* **5011**, 149–160.
6. McKeague, I. W. (2004) *J. Am. Stat. Assoc.*, in press.
7. Holmes, D. I. & Kardos, J. (2003) *Chance* **16**, 5–8.
8. Mosteller, F. & Wallace, D. L. (1984) *Applied Bayesian and Classical Inference: The Case of the Federalist Papers* (Springer, New York).
9. Binong, J. N. G. (2003) *Chance* **16**, 9–17.
10. Thisted, R. & Efron, B. (1987) *Biometrika* **74**, 445–455.
11. Friedman, R. (1997) *Who Wrote the Bible?* (Harper, San Francisco).
12. Mielke, U., ed. (1996) *Pieter Bruegel, Die Zeichnungen* (Brepols, Turnhout, Belgium).
13. Orenstein, N. M. (2001) *Pieter Bruegel the Elder* (Yale Univ. Press, New Haven, CT).
14. Orenstein, N. M. (2003) *Int. Found. Art Res. J.* **6**, 12–17.
15. Huttenlocher, D. P., Klanderman, G. A. & Rucklidge, W. J. (1993) *IEEE Trans. Pattern Anal. Machine Intell.* **15**, 850–863.
16. Cox, T. & Cox, M. (1994) *Multidimensional Scaling* (Chapman & Hall, London).
17. Shapiro, J. (1993) *IEEE Trans. Signal Processing* **41**, 3445–3462.
18. Rinaldo, R. & Calvagno, G. (1995) *IEEE Trans. Image Processing* **4**, 909–920.
19. Buccigrossi, R. W. & Simoncelli, E. P. (1999) *IEEE Trans. Image Processing* **8** (12), 1688–1701.
20. Vaidyanathan, P. P. (1987) *IEEE ASSP Magazine* **4**, 4–20.
21. Vetterli, M. (1987) *IEEE Trans. ASSP* **35**, 356–372.
22. Simoncelli, E. P. & Adelson, E. H. (1990) *Subband Image Coding* (Kluwer Norwell, Boston).